Taylor & Francis
Taylor & Francis Group

RESEARCH ARTICLE

🔓 OPEN ACCESS | Check for updates

Activity guided discovery of dual inhibitors of α-glucosidase and β-glucuronidase from the leaves of *Millettia pachycarpa* Benth

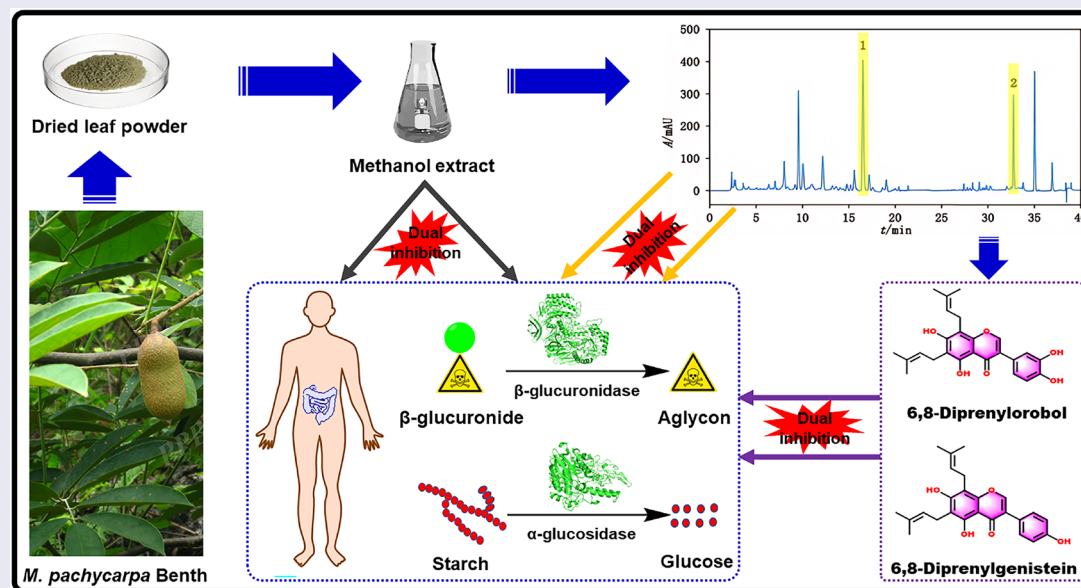Yanxi He[a‡], Huanran Xu[b‡], Shaoqian Tan[a*], Jing Long[a], Hui Lei[c], Ling Xiao[b], Xiaoyi Qi[a], Mingming Deng[a], Xia Xiong[a], Jingcan You[d], Liangliang Zhu[b], Muhan Lü[a] and Sicheng Liang[a,d]

[a]The Affiliated Hospital of Southwest Medical University, Luzhou, People's Republic of China; [b]Innovation Centre of Targeted Development of Medicinal Resources (iCTM), Anqing Normal University, Anqing, People's Republic of China; [c]School of Pharmacy, Southwest Medical University, Luzhou, People's Republic of China; [d]Basic Medicine Research Innovation Centre for Cardiometabolic Diseases, Ministry of Education, Southwest Medical University, Luzhou, China

ABSTRACT

Type 2 diabetes mellitus (T2DM) and cancers are two globally prevalent diseases which can increase the incidence of each other. Intestinal α-glucosidase and β-glucuronidase are key targets for glycaemic control and chemotherapy detoxification, respectively. This study first found that the leaf methanol extract of *Millettia pachycarpa* displayed dual inhibition to the two enzymes. The dually active constituents were then isolated and identified as two prenylated isoflavones of 6,8-diprenylorobol and 6,8-diprenylgenistein. Diprenylorobol exhibits competitive inhibition to both the two enzymes with K_i values of 21.6 μM (α-glucosidase) and 1.41 μM (β-glucuronidase). Diprenylgenistein is an uncompetitive inhibitor of α-glucosidase ($K_i = 11.4$ μM) but a competitive inhibitor of β-glucuronidase ($K_i = 1.69$ μM). Molecular docking studies showed that both the two isoflavones tightly bind into the active pockets via various hydrogen bonds and hydrophobic interactions. In summary, the current study identifies two promising dual inhibitors of α-glucosidase and β-glucuronidase from the leaves of *Millettia pachycarpa*.

GRAPHICAL ABSTRACT

CONTACT Liangliang Zhu ✉ zhuliangliang@aqnu.edu.cn 🏫 School of Life Science, Anqing Normal University, 1318 Jixianbei Road, Anqing 246133, China; Muhan Lü ✉ lvmuhan@swmu.edu.cn; Sicheng Liang ✉ liangpharm@swmu.edu.cn 🏫 The Affiliated Hospital of Southwest Medical University, Luzhou 646000, China
‡These authors contributed equally to this work.
*Co-first author.

Introduction

Type 2 diabetes mellitus (T2DM) is becoming more and more prevalent worldwide, with a 50% surge in incidence over three decades over the past three decades according to global burden of disease data[1]. Epidemiologically, T2DM is linked to increase the incidence of malignancies, including liver, pancreatic, endometrial, colorectal, and breast cancers[2,3]. Therefore, there has been growing interest in repurposing anti-diabetic drugs (e.g. metformin) in treatment of cancers[4,5]. Meanwhile, emerging evidences have indicated that cancer survivors are also at an increased risk of developing subsequent diabetes[6,7]. Irinotecan, a cornerstone for solid tumours, induces severe delayed diarrhoea in most of patients across treatment cycles, often necessitating treatment discontinuation, dose reduction, and escalated healthcare costs[8–10]. Therapeutically, dual-target agents addressing both metabolic dysregulation and chemotherapy toxicity hold promising potential.

Glycosidases represent two key targets for treatment of T2DM and chemotherapy induced toxicities, respectively. α-Glucosidase (E.C.3.2.1.20, α-GUS) modulates postprandial hyperglycaemia via oligosaccharide hydrolysis, while gut microbial β-glucuronidase (E.C.3.2.1.31, β-GUS) releases SN-38 (irinotecan's toxic metabolite) through deglucuronidation[11,12]. Clinically approved α-GUS inhibitors (acarbose and miglitol) delay glucose absorption, whereas β-GUS inhibitors (e.g. baicalin) reduce gastrointestinal exposure of SN-38[12–15]. Therapeutically, dual inhibition of α- and β-GUS could synergistically address T2DM-cancer comorbidities, surpassing single-target limitations.

Medicinal plants have long been used as alternative medicine in treating T2DM and chemotherapeutic toxicity. A variety of naturally occurring chemicals have been reported to be potent inhibitors of α-GUS or β-GUS[12,16,17]. Particularly, several flavone chemicals (e.g. baicalein and quercetin) were demonstrated to be dual inhibitors of the two enzymes[18,19]. Encouraged by these findings, this study was conducted to screen a variety of plants in hopes of discovery of dual inhibitors of α-GUS and β-GUS. We first found that the methanol leaf extracts of *Millettia pachycarpa* Benth (LMP) display inhibition towards both the two enzymes. Then, this study characterised the main active components in LMP, kinetically determined the inhibition type and inhibitory potentials, and furtherly exploring possible structural mechanism behind dual inhibition of α-GUS and β-GUS. It is hoped that the results of this study will be helpful in comorbid diabetes-chemotherapy management, as well useful in development of new naturally occurring dual inhibitors.

Materials and methods

Chemicals, enzymes, and reagents

The leaves of *Millettia pachycarpa* Benth, *Zephyranthes candida*, *Prunus subg. Cerasus sp.*, *Cerasus spp.*, *Elephantopus scaber* L., *Artemisia lactiflora* Wall. ex DC., *Cassia tora* Linn., *Ipomoea batatas* Lam., *Plantago depressa* Willd., *Lagenaria siceraria* (Molina) Standl., *Hibiscus syriacus* L., *Bauhinia purpurea* L., *Litchi chinensis* Sonn., *Ophiopogon japonicus*, *Ziziphus jujuba* Mill., *Quisqualis indica* L., *Cucurbita moschata* (Duch. ex Lam.) Duch. ex Poiret, *Hibiscus mutabilis* L., *Eremochloa ciliaris* (L.) Merr., and *Ligustrum lucidum* Ait. used in this study were obtained from Luzhou, China. 4-Nitrophenyl-α-D-glucopyranoside (PNPG) was obtained from Shanghai Macklin Biochemical Technology Co., Ltd. (Shanghai, China). 4-Methylumbelliferyl-β-D-glucuronide (4-MUG) was obtained from Shanghai Yuanye Bio-Technology Co., Ltd. (Shanghai, China).

4-Methylumbelliferone (4-MU) was purchased from Shanghai Titan Scientific Co., Ltd. (Shanghai, China). *S. cerevisiae* α-GUS, *E. coli* β-GUS, and PNP and acarbose were purchased from Sigma-Aldrich (St. Louis, MO). D-Saccharic acid 1,4-lactone (DSL) was purchased from Target Molecule Corp. (Wellesley Hills, MA). 6,8-Diprenylorobol (DPL) and 6,8-diprenylgenistein (DPG) were isolated and prepared from the extract of LMP. All reagents and solvents are of analytical or chromatographic grade. Based on analysis results by HPLC-UV, the purities of these compounds are all above 95% (Figs. S1 and S2).

Preparation of methanol plant extracts

The fresh leaves of plants were first dried and then ground into powder. The plant materials were immersed in methanol for 30 min, followed by ultrasonic extraction for another 30 min. The filtered extracts were then combined and concentrated by using a rotary evaporator at 40 °C to obtain the crude extracts, which were subsequently dissolved in methanol as stock solution (25 mg/mL) for α-GUS and β-GUS inhibition screening.

α-GUS inhibition assay

The incubation mixture was composed of PBS buffer (pH 6.8, 100 mM), α-GUS (0.1 U/mL), and PNPG in the presence or absence of different concentrations of inhibitors. To perform an accurate inhibition evaluation, preliminary kinetic assays were first conducted for the probing reaction. For PNPG hydrolysis by α-GUS, the K_m and V_{max} values were $537 \pm 76 \mu M$ and $1.05 \pm 0.03 \mu mol/min/U$, respectively. Therefore, 500 μM PNPG (a value closed to the K_m value) was used in inhibition screening and IC_{50} determinations, while 200–1500 μM PNPG (covering the K_m value) were used in inhibition constant determinations. After preincubation with α-GUS at 37 °C for 10 min, PNPG was added to initiate the hydrolysis. After incubation at 37 °C for 20 min, 0.1 M NaOH (50 μL) was added to stop the reaction. The incubation mixtures were centrifuged at $20\,000 \times g$ at 4 °C for 20 min. The supernatants (100 μL) were then transferred into the 96-well plates, and the absorption of the hydrolysis product PNP was read by microplate reader (BioTek Instruments, Inc., Winooski, VT) under the wavelength of 405 nm. Acarbose was used as a positive control inhibitor. The residual activity of α-GUS could be calculated by the following formula: residual activity (%) = (absorption of PNP in the presence of inhibitor)/absorption of PNP in the negative control (methanol only) × 100%.

β-GUS inhibition assay

Preliminary kinetic experiment assays demonstrated that the K_m and V_{max} values for 4-MUG hydrolysis by β-GUS were $102 \pm 6 \mu M$ and $7.21 \pm 0.10 \mu mol/min/mg$, respectively. The incubation mixture was composed of PBS buffer (pH 7.4, 50 mM), β-GUS (5 ng/mL), and 4-MUG (100 μM for inhibition screening; 50–2000 μM for inhibition constant determination) in the presence or absence of different concentrations of inhibitors. After incubation (200 μL) at 37 °C for 40 min, the reactions were terminated by adding 50 μL acetonitrile. Then, the incubation mixtures were centrifuged at $20\,000 \times g$ at 4 °C for 20 min to remove the protein. The supernatants (100 μL) were transferred into the 96-well plates. The fluorescence intensity of the hydrolysis product 4-MU was read by fluorescent microplate reader (BioTek Instruments, Inc., Winooski, VT) with the excitation/

emission wavelength of 360/455 nm. DSL was used as a positive control inhibitor. The residual activity of β-GUS could be calculated by the following formula: residual activity (%) = (fluorescence intensity of 4-MU in the presence of inhibitor)/(fluorescence intensity of 4-MU in the negative control) × 100%.

Chemical fingerprinting by LC-UV and fraction collection

Samples were analysed on a HPLC system (Agilent Technologies, Shanghai, China) consisting of a G7111A Quat pump VL, a G7129C Vialsampler autoinjector, a G7130A ICC heat exchanger, and a G7115A DAD WR detector to perform fingerprint analysis and LC fraction collection. The chromatographic separations were achieved using a C18 column (4.6 mm × 250 mm, 5 μm, Lubex Kromasil) at a flow rate of 1 mL/min. The column temperature was set at 30 °C. The mobile phase consisted of acetonitrile (A) and water containing 0.1% phosphoric acid (B), eluted with a long gradient: 0–15.0 min, 15–25% A; 15.0–25.0 min, 25–70% A; 25.0–39.0 min, 70–95% A. The injection volume of the methanol plant extracts was set to 2.5 μL. In the range of 0–39 min, the LC fractions of methanol plant extracts were collected consecutively every 3 min. The collections were dried by dry nitrogen blower (LICHEN, LC-DCY-24G) and then redissolved in methanol to further determine the inhibitory effect to α-GUS and β-GUS.

Identification of α-GUS and β-GUS inhibitors in the leaves of Millettia pachycarpa Benth

The major constituents of the bioactive fractions (F6, F11) of LMP were carefully analysed by a LC–MS/MS system (Shimadzu Corporation, Kyoto, Japan), which includes a LC-30AD × 2 infusion pumps, a DGU-20A5 online degasser, a SIL-30AC automatic sampling device, a CTO-20A column oven, a CBM-20A system controller, a Triple Quad tandem mass spectrometer, and a computer equipped with the LabSolutions software (ver. 5.85; Shimadzu, Kyoto, Japan). A Shim-pack C18 column (2.1 × 50 mm, 3 μm; Shimadzu, Kyoto, Japan) was utilised for chromatographic separation with the column temperature of 40 °C. The mobile phase was (A) acetonitrile and (B) ultrapure water at a flow rate of 0.3 mL/min, with the following gradient: 0–20 min, 95% B to 5% B. The optimised spectrometric conditions were set as follows: the ion spray voltage, source temperature, and desolvation temperature were 3.5 kV, 400 °C, and 200 °C, respectively. The flow rates of the atomising gas, heating gas, and drying gas were 2.5 L/min, 8.0 L/min, and 10.0 L/min, respectively. Collision energy was set at 35 eV in positive and negative ion mode. The ^{1}H NMR (500 MHz) and ^{13}C NMR (125 MHz) spectra were measured on a Varian Unity INOVA 500 spectrometer using tetramethylsilane (TMS) as an internal standard. The chemical structures of the purified compounds were elucidated through nuclear magnetic resonance (NMR) and LC–MS/MS spectra.

Inhibition kinetic analyses

Kinetic analysis was conducted for the inhibition of DPL and DPG against α-GUS and β-GUS by using PNPG (200–2000) and 4-MUG (50–2000 μM) as the substrate, respectively. Various concentrations of DPL (0–45 μM) and DPG (0–120 μM) were employed in the incubations. The Lineweaver–Burk and Dixon plots were drawn to determine the inhibition pattern of the tested inhibitor. The inhibition constant (K_i) values were calculated via fitting the equations of competitive inhibition (1), non-competitive inhibition (2),

uncompetitive inhibition (3), or mixed inhibition (4) into data. The goodness of fitting (R^2) was used to validate the most appropriate type of inhibition mechanism.

$$v = \frac{V_{max} \times [S]}{K_m \times \left(1 + \frac{[I]}{K_i}\right) + [S]} \qquad (1)$$

$$v = \frac{V_{max} \times [S]}{(K_m + [S]) \times \left(1 + \frac{[I]}{K_i}\right)} \qquad (2)$$

$$v = \frac{V_{max} \times [S]}{K_m + [S] \times \left(1 + \frac{[I]}{K_i}\right)} \qquad (3)$$

where V is the reaction rate; K_i is the inhibition constant, describing the affinity of the inhibitor to the enzyme; S and I are the concentrations of the substrate and the inhibitor, respectively; V_{max} is the maximum velocity; K_m is the substrate concentration at 0.5 V_{max}.

Molecular docking simulation

The crystal structure of β-GUS (PDB code: 3K4D) was obtained from Protein Data Bank. Since no experimental crystal structure of α-GUS is available, the structure was obtained from alpha fold 2 (https://alphafold.ebi.ac.uk/entry/P07265)[20,21]. Water molecules were removed and non-polar hydrogen atoms were added to the protein structure in PyMOL 2.4. In docking assays with α-GUS, Asp69, Tyr158, Glu277, Thr310, Ser311, Arg315, Asp352, Glu411, and Arg442 in the active site were selected as the referring amino acid residues according to the previous study[19]. Since Glu 413 was demonstrated to be a key residue in catalysing hydrolytic reaction[22], it was used as the cantered residue in docking ligands into the active pocket of β-GUS. Docking results were obtained by AutoDock 4.2 with a size of 126 × 126 × 126 Å in the x-, y, and z-axis at grid spacing, respectively. The 3D models of Acarbose, DSL, DPL, and DPG were obtained from PubChem. Ligand was converted to pdbqt format in Open Babel 2.4.1 setting. Docking results were visualised and analysed using PyMOL 2.4.

Statistical analysis

All the incubations were performed in triplicate and the data are expressed as mean ± SD. The IC$_{50}$ (half maximal inhibitory concentration) and K_i values were calculated by the nonlinear regression analysis of GraphPad Prism 7.0 (San Diego, CA).

Results

Inhibition screening of leaf extracts towards α-GUS and β-GUS

The methanol extracts of 20 plants (100 μg/mL) were evaluated for their inhibition activities towards α-GUS and β-GUS. It can be seen from Figure 1 that the activities of the two enzymes were both inhibited by the extract of LMP, with the residual activities of

45.67% (α-GUS) and 7.00% (β-GUS). Further inhibition assays indicate that the methanol extract of LMP could dose-dependently reduce activities of α-GUS and β-GUS with IC$_{50}$ values of 98.80 ± 9.53 μg/mL and 16.01 ± 1.98 μg/mL, respectively (Figure 2). These results strongly suggest that the methanol extract of LMP contains naturally occurring α-GUS and β-GUS inhibitors.

Identification of α-GUS and β-GUS inhibitors from LMP

In order to discover the naturally occurring inhibitors from LMP, the extract was first separated into 13 fractions by HPLC (Figure 3). The eluted fractions were collected, concentrated, and evaluated for their inhibiting activities towards α-GUS and β-GUS. As illustrated in Figure 3(B), fractions 6 and 11 exhibited potent inhibition towards α-GUS, reducing residual enzyme activity to below 50%, while other fractions showed minimal inhibitory effects. For β-GUS, fractions 6, 7, 10, 11, and 12 reduced enzymatic activity to below 50% of control levels, whereas fractions 2 and 13 demonstrated mild stimulatory effects, and remaining fractions exerted negligible effects. Of the tested fractions, only fractions 6 and 11 displayed dual inhibition towards the two glycosidases. In the MS/MS spectra, fraction 6 displayed molecular ion peaks at *m/z* 423.2 (negative-ion mode) and 424.2 (positive-ion mode) (Fig. S3), while fraction 11 exhibited peaks at *m/z* 407.2 (negative-ion mode) and 405.2 (positive-ion mode) (Fig. S4). After comparing the NMR
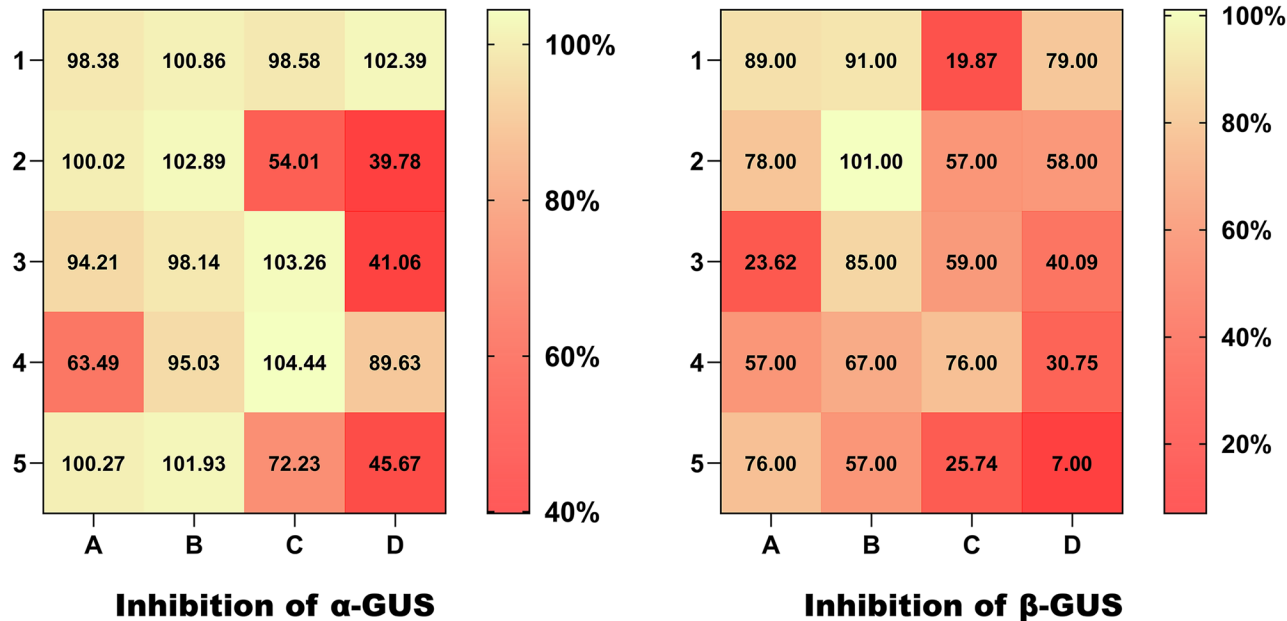

Figure 1. Inhibition of α-GUS and β-GUS by methanol extracts (100 μg/mL) of leaves of 20 plants. Data represent the mean residual activities of the triplicate determinations. A1: *Zephyranthes candida*; A2: *Prunus subg. Cerasus sp*; A3: *Cerasus spp.*; A4: *Elephantopus scaber* L.; A5: *Artemisia lactiflora* Wall. ex DC.; B1: *Cassia tora* Linn.; B2: *Ipomoea batatas* (L.) Lam.; B3: *Plantago depressa* Willd.; B4: *Lagenaria siceraria* (Molina) Standl.; B5: *Hibiscus syriacus* L.; C1: *Bauhinia purpurea* L.; C2: *Litchi chinensis* Sonn.; C3: *Ophiopogon japonicus*; C4: *Ziziphus jujuba* Mill.; C5: *Quisqualis indica* L.; D1: *Cucurbita moschata* (Duch. ex Lam.); D2: *Hibiscus mutabilis* L.; D3: *Eremochloa ciliaris* (L.) Merr.; D4: *Ligustrum lucidum* Ait.; D5: *Millettia pachycarpa* Benth.
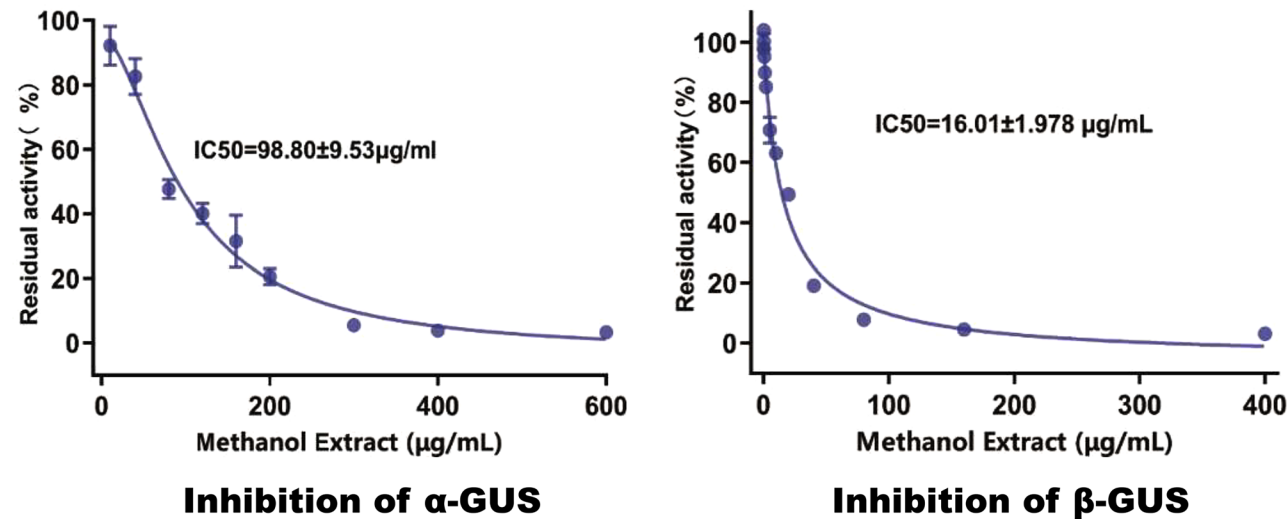

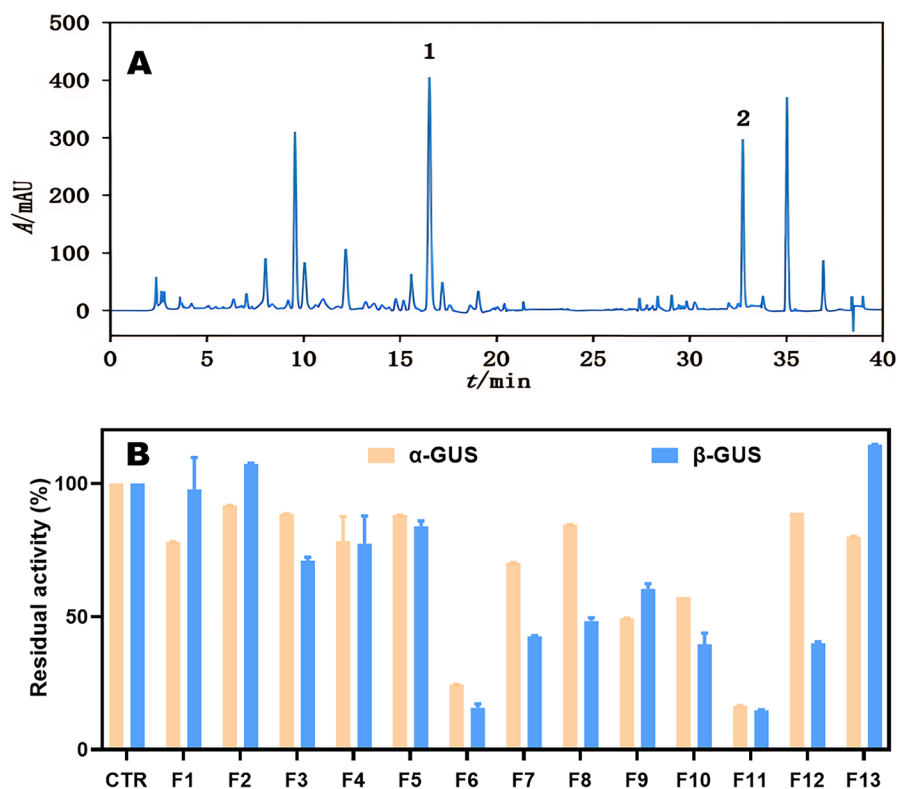**Figure 2.** Dose-dependent inhibition of α-GUS and β-GUS by the methanol extracts of leaves of *Millettia pachycarpa* Benth (LMP). Data points represent the mean residual activities of the triplicate determinations, and error bars are the calculated SD values.

Figure 3. LC-UV fingerprinting of the leaves of *Millettia pachycarpa* Benth extract (A); inhibition of α-GUS and β-GUS by the LC fractions (F1–F13) collected at 3 min intervals (B). Each data column and error bar represent as the mean and SD of triplicate determinations. Methanol was used as the negative control (CTR).
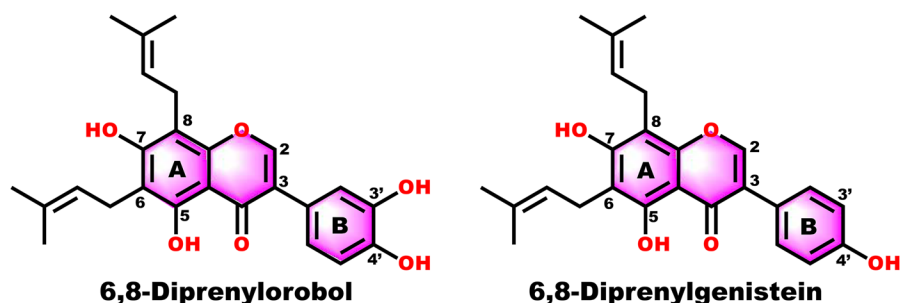
Figure 4. Molecular structures of 6,8-diprenylorobol (DPL) and 6,8-diprenylgenistein (DPG).

(Figs. S5 and S6) with the reported phytochemical studies[22,23], the key constituents in fractions 11 and 6 were characterised as DPL and DPG (Figure 4), respectively. It is anticipated that DPL and DPG may both act as dual inhibitors of α-GUS and β-GUS.
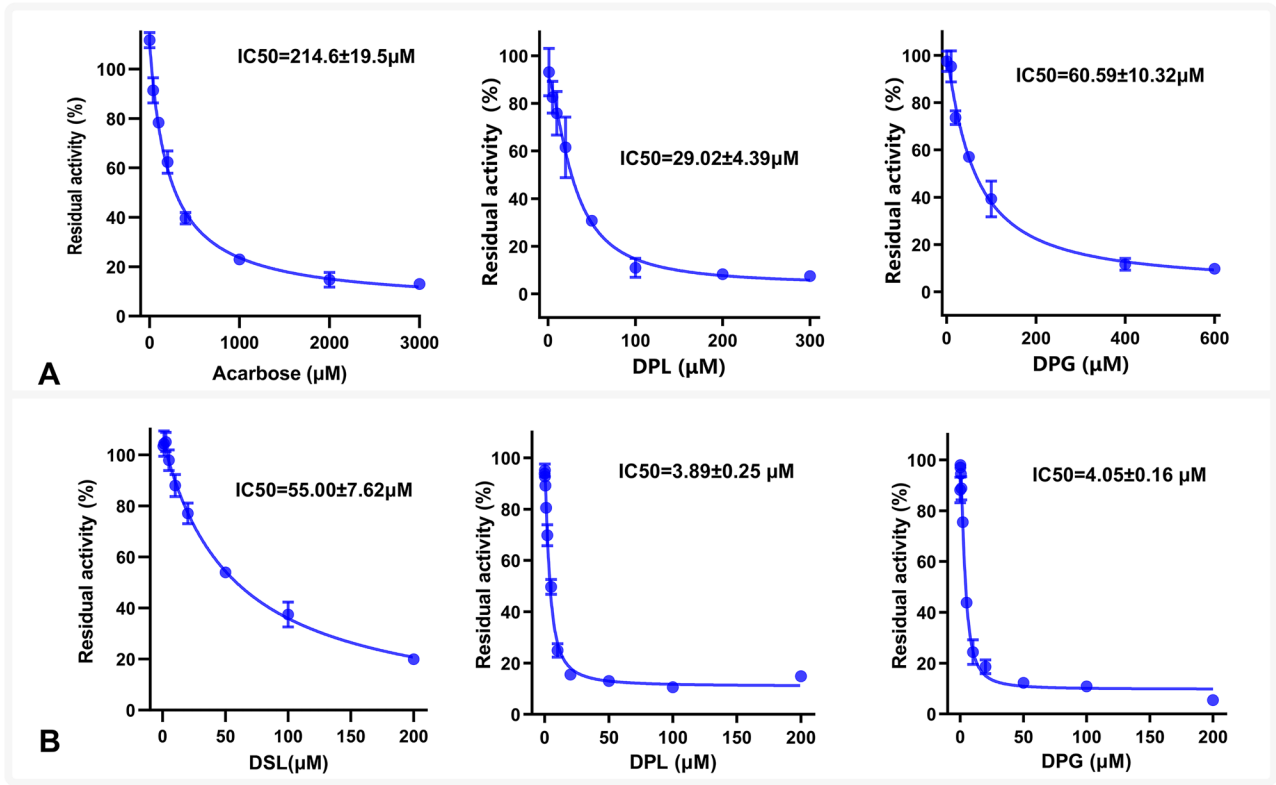
Inhibition of α-GUS and β-GUS

In a similar way to the methanol extract of LMP, DPL and DPG could both dually inhibit α-GUS and β-GUS in a dose-dependent manner (Figure 5). Figure 5 also indicates that DPL and DPG both display stronger inhibition than the positive control inhibitors (DSL and acarbose). The IC_{50} values for inhibition of α-GUS by DPL and DPG were dozens of μM, while the values for inhibition of β-GUS were just a few μM (Table 1). Consistently, the leaf extract also displayed stronger inhibition to β-GUS than to α-GUS (Table 1). Based on these results, it can be concluded that DPL and DPG are responsible for dual inhibition of α-GUS and β-GUS by the extract of LMP.

Kinetic analyses for inhibition of α-GUS and β-GUS

To get a more accurate evaluation of the inhibitory potency, kinetic analyses were performed to obtain information related to inhibition types and the corresponding K_i values. With respect to inhibition of α-GUS, the Lineweaver–Burk plot (1/v vs. 1/[PNPG]) indicates that DPL shows competitive inhibition that is consistent with the Dixon plot (1/v vs. [DPL]) (Figure 6(A)). Nonlinear regression analysis confirms that DPL inhibits the enzyme obeying competitive inhibition model (Equation (1), R^2 = 0.96) with the K_i value calculated to be 21.6 ± 2.3 μM. As can be seen from Figure 6(B), DPG acts as an uncompetitive inhibitor which is different from DPL. The K_i value was calculated to be 11.4 ± 2.2 μM via fitting data into the uncompetitive inhibition model (Equation (3), R^2 = 0.98).

With respect to inhibition of β-GUS, the linear kinetic plots (Figure 7) lead to a conclusion that DPL and DPG act as a competitive and non-competitive inhibitor, respectively. Fitting kinetic data into competitive inhibition model (Equation (1), DPL) and non-competitive inhibition model (Equation (2), DPG) yield

Figure 5. Dose-dependent inhibition of α-GUS (A) and β-GUS (B) by DPL, DPG, and the positive control inhibitors (acarbose and DSL, respectively). Each data point and column represent as the mean of triplicate determinations, and the error bars are the calculated SD values.

Table 1. IC_{50} and K_i values for the inhibition of α-GUS and β-GUS by the methanol extract of leaves of *Millettia pachycarpa* Benth, 6,8-diprenylorobol (DPL), 6,8-diprenylgenistein (DPG), and the known positive inhibitors (acarbose and DSL).

Inhibitors	Enzyme	Substrates	IC_{50}	K_i (µM)	Inhibition type
Extract	α-GUS	PNPG	98.8 ± 9.5	NA	NA
	β-GUS	4-MUG	16.0 ± 2.0	NA	NA
DPL	α-GUS	PNPG	29.0 ± 4.4	21.6 ± 2.3	Competitive
	β-GUS	4-MUG	3.89 ± 0.25	1.41 ± 0.18	Competitive
DPG	α-GUS	PNPG	60.6 ± 10.3	11.4 ± 2.2	Un-competitive
	β-GUS	4-MUG	4.05 ± 0.16	2.62 ± 0.10	Non-competitive
Acarbose[a]	α-GUS	PNPG	215 ± 20	ND	ND
DSL[a]	β-GUS	4-MUG	55.0 ± 7.6	ND	ND

NA: not applicable; ND: not determined.
[a]Positive control inhibitors.
IC_{50} values for leaf extract are in µg/mL, while the values for the other inhibitors are in µM.

K_i values of 1.41 ± 0.18 µM (R^2 = 0.96) and 2.62 ± 0.10 µM (R^2 = 0.99), respectively. It is demonstrated that DPL is more effective in inhibiting β-GUS.

## Molecular docking simulations

In order to decipher structural mechanism for dual inhibition of α-GUS and β-GUS, docking analyses were conducted for DPL and DPG (as well as the positive control inhibitors), respectively. The results revealed that DPL and DPG could interact with the amino acid residues in the catalytic cavities of both the two enzymes. The binding energies for DPL and DPG bound to α-GUS were −9.41 kcal/mol and −8.85 kcal/mol, while the energy for acarbose bound was −5.13 kcal/mol. The control docking suggests that

acarbose can form 10 hydrogen bonds with six amino residues, including Phe157, His239, Glu304, Thr307, Pro309, Phe310, and Arg312 (Figure 8(A)). As shown in Figure 8(B,C), the skeletal structure of isoflavone (A and B rings) can form various hydrogen bonds and hydrophobic interactions with multiple amino acid residues in the active pocket. The two prenyl groups can form additional hydrophobic interactions with the amino acid residues. Interestingly, there is no hydrogen bond formation with C7-OH in the "A ring", and the presence of C5-OH even results in unfavourable donor–donor interaction. In contrast, both C3'-OH and C4'-OH in the C ring are favoured by α-GUS binding the two prenylated isoflavones.

Docking analysis indicates that the binding energies for DPL and DPG bound to β-GUS are −6.99 and −7.09 kcal/mol, while the energy for DSL bound was −3.39 kcal/mol. As shown in Figure 9(A), the known inhibitor DSL can form eight hydrogen bonds with eight amino acid residues, including Asp163, Asn412, Glu413, Asn466, Tyr472, Trp549, Arg562, and Asn566. Figure 9(B,C) indicates that the two prenyl groups contribute significantly to DPL and DPG bound via hydrophobic interactions. Figure 9(B,C) also indicates that multiple amino acid residues (Asp163, Leu361, Tyr472, Arg562) are shared by the two inhibitors. It is additionally demonstrated that Glu413, a key residue in catalysing hydrolytic reaction, involves in interaction with DPL and DSL other than DPG. There is no interaction between C7-OH with the activity pocket of β-GUS, which resembles interactions with α-GUS.

Discussion

It has been documented that T2DM and malignancies can increase the incidence of each other. This pathophysiological interplay
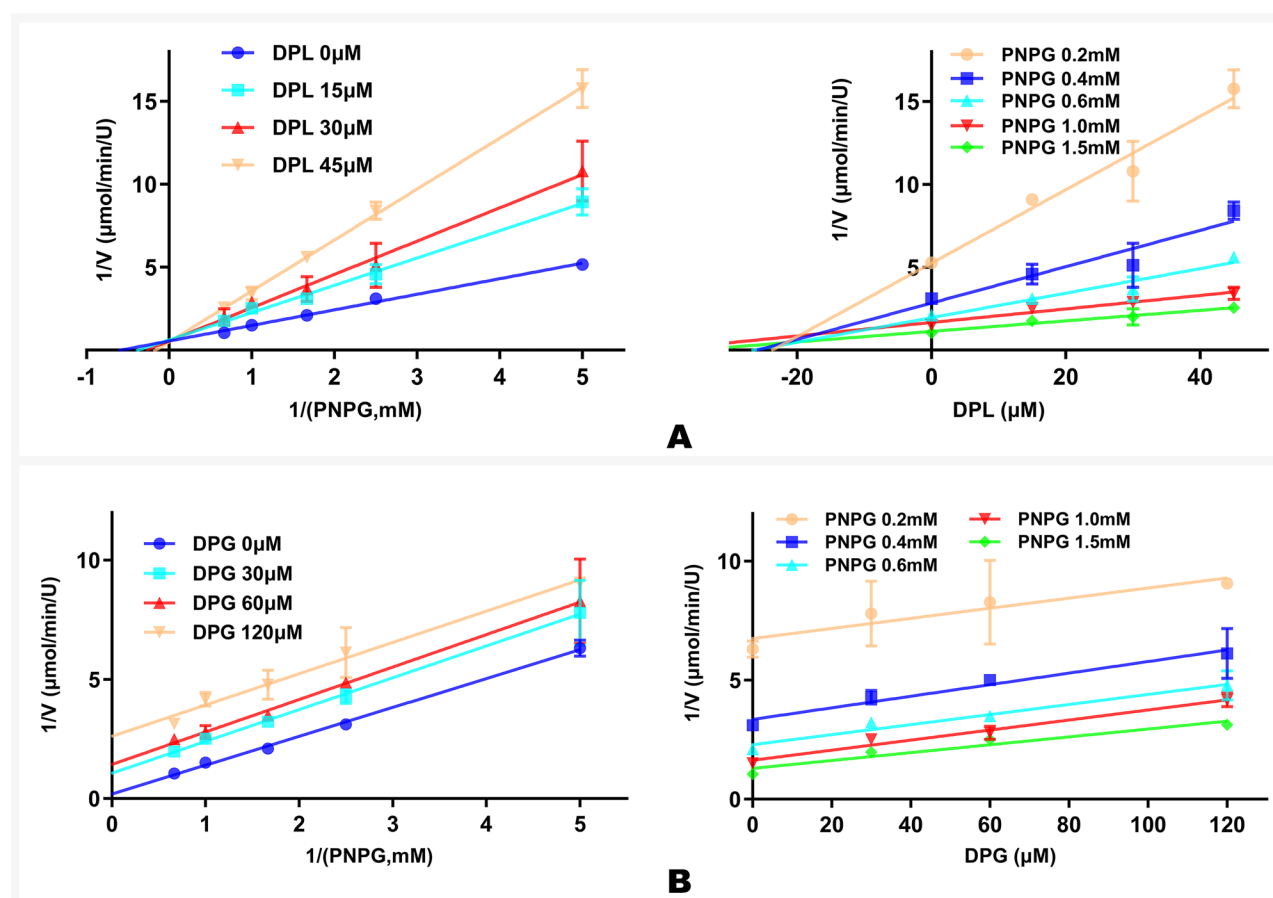
Figure 6. The Lineweaver–Burk and Dixon plots for inhibition of α-GUS by DPL (A) and DPG (B). The data points represent as the mean of the triplicate determinations, and the error bars represent the calculated SD values.

highlights the therapeutic value of dual-targeting therapies that simultaneously address both diseases. Notably, α-GUS is a well-established pharmacological target for T2DM management, whereas β-GUS activity has been implicated in aggravating chemotherapy-induced gastrointestinal toxicity. While α-GUS inhibitors are clinically approved for blood glucose regulation, β-GUS inhibitors are active in mitigating adverse gastrointestinal effects associated with specific chemotherapeutic regimens. Guided by the inhibitory activities, we identified two novel dual inhibitors (DPL and DPG) of α-GUS and β-GUS in the methanol extract of LMP.

M. pachycarpa is an ethnomedicinal plant distributed throughout Southeast Asia which has gain wide applications in clinic, agriculture, and fishery [24]. In clinical practise, botanical extracts of different parts are used locally in treatment of infertility, inflammation, cancer, and insect infections[24]. Our current study revealed that the methanolic extract of leaves demonstrates potent inhibition against both α-GUS and β-GUS, with IC_{50} values of 0.1 mg/mL and 0.02 mg/mL, respectively (Table 1). It was previously reported that this extract (0.1 mg/mL) displayed anti-inflammatory effect as determined by *in vitro* human red blood cell stability method[25]. Meanwhile, the extract was active in scavenging of radicals by 2,2-diphenyl-1-picrylhydrazyl assay with the EC50 value of about 0.2 mg/mL[26]. Moreover, the root methanol extract (5 mg/mL) displayed anthelmintic activity against intestinal parasitic roundworms *Raillietina echinobothrida* and *Ascaridia galli*[27,28]. Compared to other documented pharmacological activities, inhibition of β-GUS and α-GUS may occur at substantially lower concentrations. Through activity-guided fractionation, the two prenylated isoflavones DPL and DPG were identified as the principal dual inhibitors in LMP. The two compounds have been previously characterised in the trichloromethane extract of aerial parts and the ethyl acetate extract of leaves[29,30].

The current study indicates that DPL and DPG exhibit superior α-GUS inhibitory efficacy compared to the clinical reference drug acarbose, which is in consistent with the previous studies[30–32]. The two prenylated isoflavones DPL and DPG may act as promising candidates for developing next-generation hyperglycaemia therapeutics. Notably, DPG demonstrates a multi-target pharmacological profile beyond α-GUS inhibition. It was reported to be an inhibitor α-amylase with the IC_{50} value of 14.8 μM, suggesting another way impeding starch hydrolysis[30]. Though inhibition of protein tyrosine phosphatase-1B (IC_{50} = 2.3–28 μM), it enhances tyrosine phosphorylation and thereby promoting insulin signalling[32,33]. In addition, DPG (>10 μM) could effectively increase both of the basal and insulin-stimulated glucose uptake in L6 myotubes[33]. Moreover, DPG (>2.5 μM) is able to reverse the high glucose induced injury in human umbilical vein endothelial cells[34]. These mechanistically distinct yet synergistic actions suggest that DPG may act as a multi-faceted therapeutic agent for T2DM, potentially addressing both glycaemic control and diabetic complications.

The current study additionally demonstrates that DPL and DPG act as potent inhibitors of β-GUS (Table 1). This finding holds particular clinical relevance, as β-GUS inhibition has been clinically validated to alleviate severe gastrointestinal tract toxicities in colorectal cancer patients receiving irinotecan therapy[12,35]. When considering
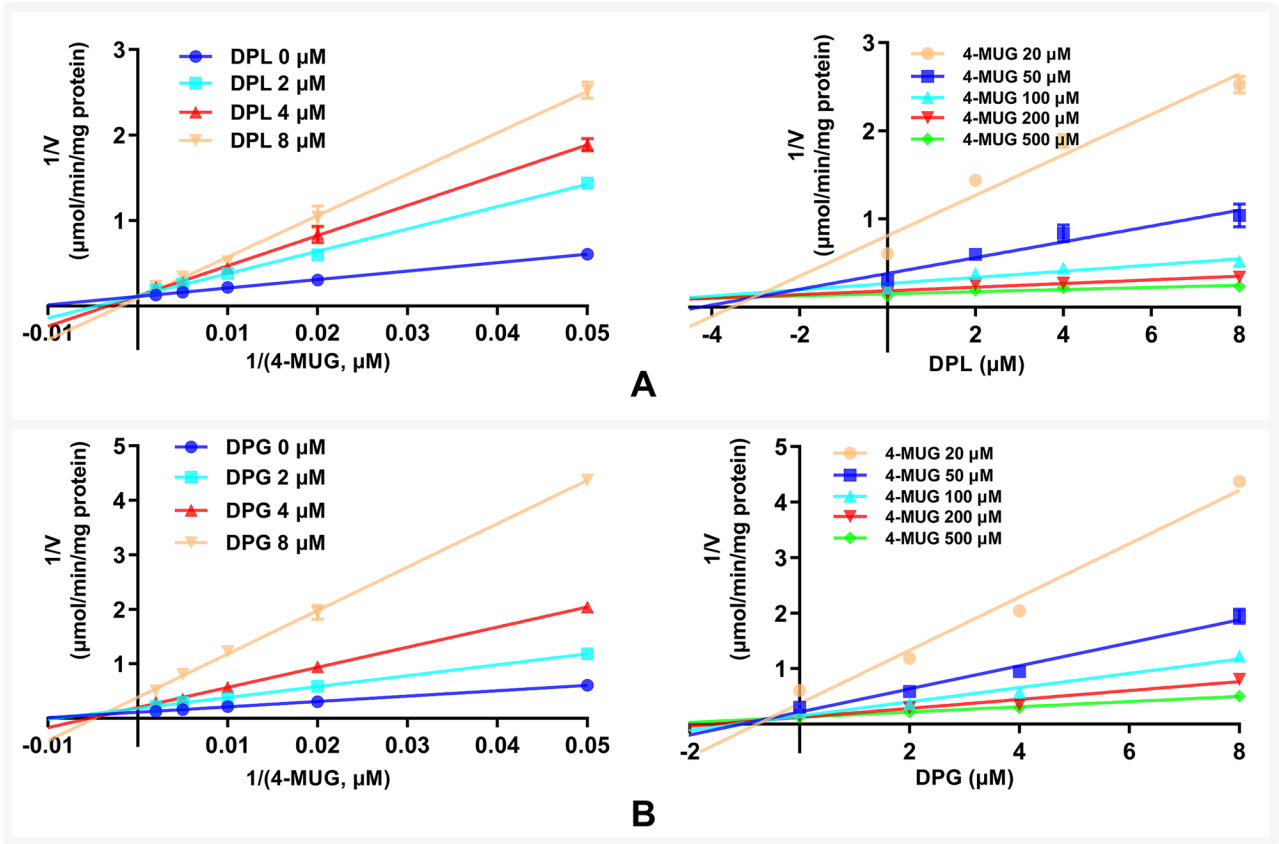
Figure 7. The Lineweaver–Burk plots and the Dixon plots for inhibition of β-GUS by DPL (A) and DPG (B). The data points represent the mean of the triplicate determinations, and the error bars represent the calculated SD values.
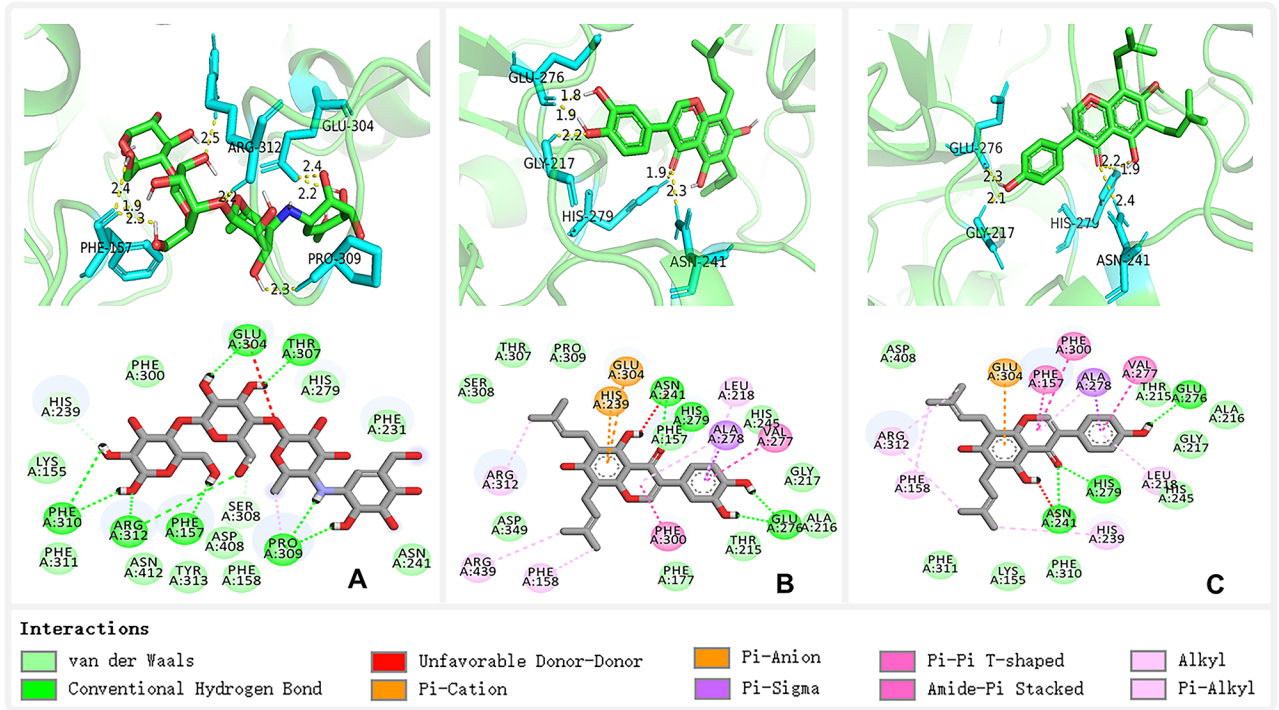
Figure 8. 3D and 2D binding interactions of acarbose (A), DPL (B), and DPG (C) with the active cavity of α-GUS.
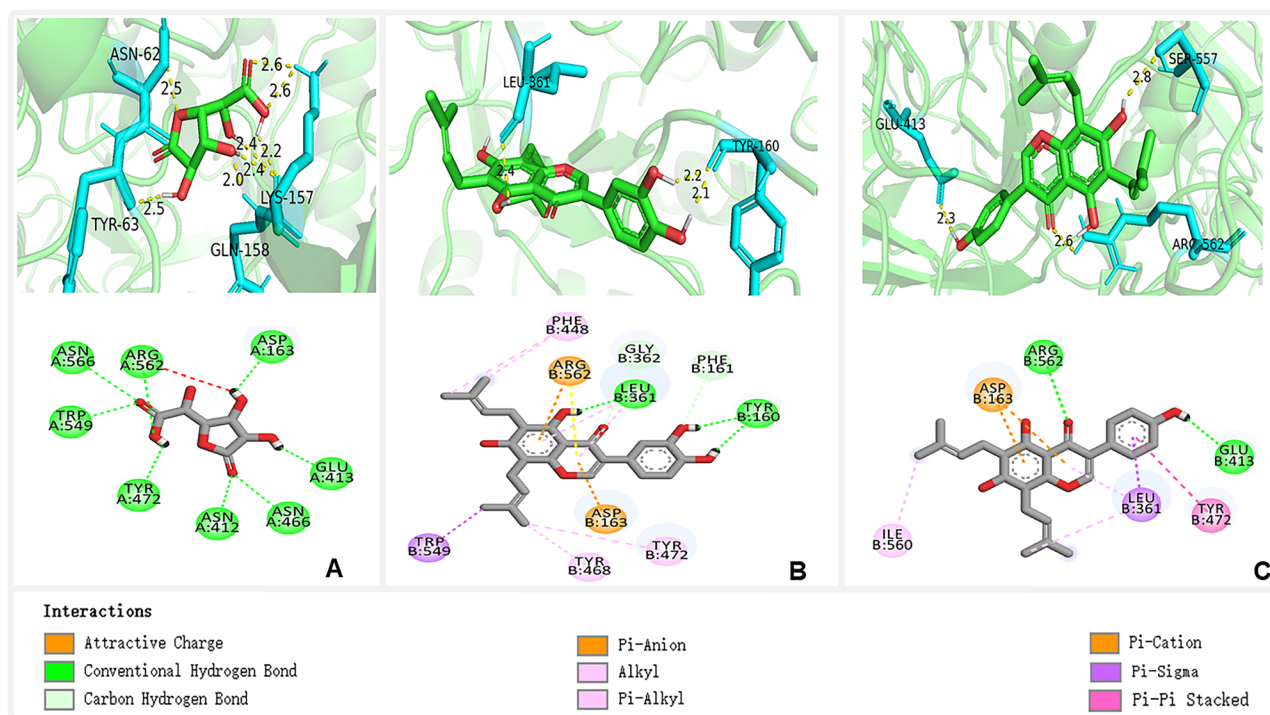
Figure 9. 3D and 2D interaction patterns of DSL (A), DPL (B), and DPG (C) with the active cavity of β-GUS.

their gastrointestinal protective potential, these isoflavones likely exert multiple synergistic actions. Both the two phytochemicals are able to scavenge radicals in ABTS assay, neutralising reactive oxygen species (ROS) in inflammatory bowel microenvironments[23]. DPG could inhibit activity of platelet-activating factor acetyltransferase (IC$_{50}$ = 19 μM), disrupting pro-inflammatory lipid mediator synthesis[36]. Meanwhile, both the two chemicals display desired anticancer activities. It was reported that DPL (40 μM) could inhibit the proliferation of human colon cancer cells via activation of p53 and generation of ROS[37]. DPG (7.1 μM) could trigger dual apoptosis and autophagy of colorectal cancer cells[38]. Through multiple synergistic actions of β-GUS inhibition, anti-inflammation, and tumour suppression, the two compounds may enhance chemotherapy tolerability while counteracting colorectal carcinogenesis.

As demonstrated in Table 1, IC$_{50}$ and K_i values for inhibition of β-GUS are much lower than those for inhibition of α-GUS. It is indicated that β-GUS is more sensitive to DPL and DPG. However, it does not mean that the therapeutic effects from inhibition of β-GUS are more readily due to distinct anatomical requirements. To alleviate the gastrointestinal toxicity, β-GUS throughout the whole gut lumen needs to be inhibited. However, to inhibit starch digestion, only duodenum α-GUS needs to be inhibited[39]. Given that the volume of duodenum lumen is much lower than the whole gut lumen, the concentrations of DPL and DPG in duodenum lumen may be much higher. It is therefore the oral dosages of the dual inhibitors may be comparable in the cases of achieving a hypoglycaemic effect and protecting colon from the gastrointestinal toxicity.

To reveal the possible structural mechanism behind the dual inhibition, the inhibitors were docked into the active pockets of a predicted α-GUS model (https://alphafold.ebi.ac.uk/entry/P07265) and a crystal structure of β-GUS, respectively[20,21,40]. To validate the docking protocol, known inhibitors (acarbose and DSL) were docked into the glycosidases' active sites as control docking assays. Acarbose can form various hydrogen bonds with multiple amino

acid residues in the active pocket of α-GUS (Figure 8(A)). This is in consistent with previous studies in which acarbose can form 12 hydrogen bonds with the enzyme[19,41]. Similarly, in docking analysis with β-GUS, the diagram of the active site with DSL bound (Figure 9(A)) is very close to the experimental determinations[40]. Moreover, binding energies for DPL and DPG bound are all lower than the positive inhibitors bound, which is highly consistent with the two isoflavones displaying much stronger inhibition. Together, these results suggest that docking analyses using both predicted and experimental structural models provide insights into DPL and DPG interaction patterns with the two glycosidases.

Historically, isoflavones have been recognised as relatively weak inhibitors of both α-GUS and β-GUS. For instance, daidzein, a representative naturally occurring isoflavone, exhibits the IC$_{50}$ values exceeding 100 μM against both of the two enzymes[18,19]. Consequently, the development of isoflavone-based inhibitors has drawn few attentions, which is in sharp contrast to the extensive exploration of flavones as potent inhibitors. Our findings reveal that the introduction of two prenyl groups at the C8 position of the isoflavone A-ring confers remarkable inhibitory potency against both α-GUS and β-GUS. Molecular docking analyses (Figures 8 and 9) confirm that the prenyl substituents form hydrophobic interactions within the catalytic pockets of both enzymes, significantly enhancing binding affinity. Intriguingly, docking assays reveal that the C7-hydroxyl group on the A-ring does not participate in molecular interactions with either enzyme (Figures 8 and 9), contrasting sharply with established structure–activity relationship paradigms for flavone inhibitors. In flavone derivatives, retention of the C7-hydroxyl group in the "A ring" is crucial for inhibition of both the two enzymes[18,19]. It appears to be that dual inhibition of α-GUS and β-GUS favours a hydrophobic "A ring" in isoflavones, while favouring a polar one in flavones.

As shown in Figure 4, isoflavones DPL and DPG exhibit a subtle structural variation: C3'-OH is present in the B ring in DPL but absent in DPG. However, this structural distinction drives differential

enzyme selectivity. According to the K_i values, DPG displays twofold stronger binding affinity with α-GUS, whereas DPL demonstrates superior β-GUS binding affinity. Previous studies related to flavone inhibitors demonstrated that B-ring ortho-dihydroxylation enhances α-GUS inhibition, while mono-hydroxylated analogues preferentially inhibit β-GUS[18,19]. It seems that α-GUS and β-GUS favour isoflavone inhibitors with different B rings, of which the molecular recognition strategies are conserved across flavonoid subclasses. We acknowledge that the interaction patterns identified here derive from analysis of only two prenylated isoflavones. To establish a robust structure–activity relationship, testing additional analogues would be required.

Conclusions

In conclusion, this study demonstrates that LMP displays inhibitory effects towards both α-GUS and β-GUS. The main active ingredients have been identified as two prenylated isoflavones DPL and DPG, both of which act as potent dual inhibitors. These findings offer an herb candidate and two leading compounds for mitigating irinotecan-induced gastrointestinal toxicity in T2DM patients undergoing chemotherapy.

Author contributions

Yanxi He and Huanran Xu: conceptualisation, methodology, formal analysis, investigation, writing-original draft, and visualisation. Shaoqian Tan and Long Jing: data curation, software, visualisation, and validation. Hui Lei, Ling Xiao, and Xiaoyi Qi: formal analysis, methodology, resources, and reviewing. Mingming Deng and Xia Xiong: methodology, visualisation, and writing-original draft. Jingcan You: data interpretation, funding acquisition, and reviewing. Liangliang Zhu, Muhan Lv, and Sicheng Liang: conceptualisation, funding acquisition, project administration, supervision, and writing-review and editing. All the authors approve the version of the manuscript to be published.

Ethical approval

The plant material of *Prunus spp.* (cultivated) used in this study was collected in accordance with the ethical guidelines of the School of Pharmacy, Southwest Medical University, as well as relevant national and international regulations. All necessary collection permits were obtained, and the collection practices fully comply with local laws and regulations. The specimens of plants in this study were identified by Professor Bing He from the School of Pharmacy, Southwest Medical University. Details of the identification and records of the specimens are maintained in the ethical approval files for this study. All specimens have been deposited in a public herbarium for further research and verification. This study ensures full compliance with applicable ethical standards and has undergone thorough legal and ethical reviews concerning the collection, use, and storage of plant samples.

Disclosure statement

The authors report no conflicts of interest.

Funding

Data availability statement

The datasets generated during the current study are available from the corresponding authors (Zhu L., Lv M., and Liang S.) on reasonable request.

References

1. Tinajero MG, Malik VS. An update on the epidemiology of type 2 diabetes: a global perspective. Endocrinol Metab Clin North Am. 2021;50(3):337–355.
2. Shlomai G, Neel B, LeRoith D, Gallagher EJ. Type 2 diabetes mellitus and cancer: the role of pharmacotherapy. J Clin Oncol. 2016;34(35):4261–4269.
3. Pearson-Stuttard J, Papadimitriou N, Markozannes G, Cividini S, Kakourou A, Gill D, Rizos EC, Monori G, Ward HA, Kyrgiou M, et al. Type 2 diabetes and cancer: an umbrella review of observational and Mendelian randomization studies. Cancer Epidemiol Biomarkers Prev. 2021;30(6):1218–1228.
4. Yang J, Zhou Y, Xie S, Wang J, Li Z, Chen L, Mao M, Chen C, Huang A, Chen Y, et al. Metformin induces ferroptosis by inhibiting UFMylation of SLC7A11 in breast cancer. J Exp Clin Cancer Res. 2021;40(1):206.
5. Hua Y, Zheng Y, Yao Y, Jia R, Ge S, Zhuang A. Metformin and cancer hallmarks: shedding new lights on therapeutic repurposing. J Transl Med. 2023;21(1):403.
6. Jordt N, Kjærgaard KA, Thomsen RW, Borgquist S, Cronin-Fenton D. Breast cancer and incidence of type 2 diabetes mellitus: a systematic review and meta-analysis. Breast Cancer Res Treat. 2023;202(1):11–22.
7. Singh S, Earle CC, Bae SJ, Fischer HD, Yun L, Austin PC, Rochon PA, Anderson GM, Lipscombe L. Incidence of diabetes in colorectal cancer survivors. J Natl Cancer Inst. 2016;108(6):djv402.
8. Kciuk M, Marciniak B, Kontek R. Irinotecan—still an important player in cancer chemotherapy: a comprehensive overview. Int J Mol Sci. 2020;21(14):4919.
9. Bailly C. Irinotecan: 25 years of cancer treatment. Pharmacol Res. 2019;148:104398.
10. Xu S, Lan H, Huang C, Ge X, Zhu J. Mechanisms and emerging strategies for irinotecan-induced diarrhea. Eur J Pharmacol. 2024;974:176614.
11. Hossain U, Das AK, Ghosh S, Sil PC. An overview on the role of bioactive α-glucosidase inhibitors in ameliorating diabetic complications. Food Chem Toxicol. 2020;145:111738.
12. Awolade P, Cele N, Kerru N, Gummidi L, Oluwakemi E, Singh P. Therapeutic significance of β-glucuronidase activity and its inhibitors: a review. Eur J Med Chem. 2020;187:111921.
13. Altay M. Acarbose is on stage again. World J Diabetes. 2022;13(1):1–4.
14. Scott LJ, Spencer CM. Miglitol: a review of its therapeutic potential in type 2 diabetes mellitus. Drugs. 2000;59(3):521–549.
15. Teng X, Wu B, Liang Z, Zhang L, Yang M, Liu Z, Liang Q, Wang C. Three bioactive compounds from Huangqin decoction ameliorate Irinotecan-induced diarrhea via dual-targeting of *Escherichia coli* and bacterial β-glucuronidase. Cell Biol Toxicol. 2024;40(1):88.

16. Ramadaini T, Sumiwi SA, Febrina E. The anti-diabetic effects of medicinal plants belonging to the Liliaceae family: potential alpha glucosidase inhibitors. Drug Des Devel Ther. 2024;18:3595–3616.

17. Kashtoh H, Baek KH. Recent updates on phytoconstituent alpha-glucosidase inhibitors: an approach towards the treatment of type two diabetes. Plants. 2022;11(20):2722.

18. Weng Z-M, Wang P, Ge G-B, Dai Z-R, Wu D-C, Zou L-W, Dou T-Y, Zhang T-Y, Yang L, Hou J, et al. Structure–activity relationships of flavonoids as natural inhibitors against *E. coli* β-glucuronidase. Food Chem Toxicol. 2017;109(Pt 2):975–983.

19. Jia Y, Ma Y, Cheng G, Zhang Y, Cai S. Comparative study of dietary flavonoids with different structures as α-glucosidase inhibitors and insulin sensitizers. J Agric Food Chem. 2019;67(37):10521–10533.

20. Varadi M, Bertoni D, Magana P, Paramval U, Pidruchna I, Radhakrishnan M, Tsenkov M, Nair S, Mirdita M, Yeo J, et al. AlphaFold protein structure database in 2024: providing structure coverage for over 214 million protein sequences. Nucleic Acids Res. 2024;52:D368–D375.

21. Jumper J, Evans R, Pritzel A, Green T, Figurnov M, Ronneberger O, Tunyasuvunakool K, Bates R, Žídek A, Potapenko A, et al. Highly accurate protein structure prediction with AlphaFold. Nature. 2021;596(7873):583–589.

22. Ahn S-J, Park S-N, Lee YJ, Cho E-J, Lim YK, Li XM, Choi M-H, Seo Y-W, Kook J-K. In vitro antimicrobial activities of 1-methoxyficifolinol, licorisoflavan A, and 6,8-diprenylgenistein against *Streptococcus mutans*. Caries Res. 2015;49(1):78–89.

23. Uddin GM, Lee HJ, Jeon JS, Chung D, Kim CY. Isolation of prenylated isoflavonoids from *Cudrania tricuspidata* fruits that inhibit A2E photooxidation. Nat Prod Sci. 2011;17(3):206–211.

24. Roy B, Bharti RR. *Millettia pachycarpa* Benth: a herbal medicinal plant of Southeast Asia. Singapore: Springer; 2020.

25. Chowdhury A, Mamun AA, Rahman S, Azam S, Shams K, Jainul A. Human red blood cell membrane stability testing for the estimation of anti-inflammatory activity of methanolic extract of *Millettia pachycarpa* Benth leaves. Int J Pharm Sci Res. 2020;7(2):4587–4590.

26. Azam S, Ansari P, Rashid MMU, Alam MN, Ahmed IH, Ibarahim MY, Shafi SM, Rahman S, Hossen A. In vitro anti-oxidant and in vivo anti-inflammatory activity determination of the methanolic leaves extract of *Millettia pachycarpa*. Biomed Res Ther. 2015;2(10):366–373.

27. Giri BR, Roy B, Sinha Babu SP. Evidence of apoptosis in *Raillietina echinobothrida* induced by methanolic extracts of three traditional medicinal plants of Northeast India. Exp Parasitol. 2013;134(4):466–473.

28. Lalchhandama K. Anthelmintic activity of *Millettia pachycarpa* root bark extract on an intestinal roundworm, *Ascaridia galli*. Pharmacogn J. 2019;11(6s):1428–1433.

29. Singhal AK, Sharma RP, Thyagarajan G, Herz W, Govindan SV. New prenylated isoflavones and a prenylated dihydroflavonol from *Millettia pachycarpa*. Phytochemistry. 1980;19(5):929–934.

30. Suthiphasilp V, Rujanapun N, Kumboonma P, Chaiyosang B, Tontapha S, Maneerat T, Patrick BO, Andersen RJ, Duangyod T, Charoensup R, et al. Antidiabetic and cytotoxic activities of rotenoids and isoflavonoids isolated from *Millettia pachycarpa* Benth. ACS Omega. 2022;7(28):24511–24521.

31. Jo YH, Lee S, Yeon SW, Turk A, Lee JH, Hong S-M, Han YK, Lee KY, Hwang BY, Kim SY, et al. Anti-diabetic potential of *Maclura tricuspidata* leaves: prenylated isoflavonoids with α-glucosidase inhibitory and anti-glycation activity. Bioorg Chem. 2021;114:105098.

32. Fan J-R, Kuang Y, Dong Z-Y, Yi Y, Zhou Y-X, Li B, Qiao X, Ye M. Prenylated phenolic compounds from the aerial parts of *Glycyrrhiza uralensis* as PTP1B and α-glucosidase inhibitors. J Nat Prod. 2020;83(4):814–824.

33. Lee MS, Kim CH, Hoang DM, Kim BY, Sohn CB, Kim MR, Ahn JS. Genistein-derivatives from *Tetracera scandens* stimulate glucose-uptake in L6 myotubes. Biol Pharm Bull. 2009;32(3):504–508.

34. Zhang X, Hao X, Chen X, Wang F, Guo H. The beneficial effects of the active components from *Maclura tricuspidata* fruits in the treatment of diabetes mellitus. Nat Prod Res. 2024;38(21):3831–3835.

35. Wang C, Teng X, Wang C, Liu B, Zhou R, Xu X, Qiu H, Fu Y, Sun R, Liang Z, et al. Insight into the mechanism of Xiao–Chai–Hu–Tang alleviates irinotecan-induced diarrhea based on regulating the gut microbiota and inhibiting Gut β-GUS. Phytomedicine. 2023;120:155040.

36. Nagumo S, Fukuju A, Takayama M, Nagai M, Yanoshita R, Samejima Y. Inhibition of lysoPAF acetyltransferase activity by components of licorice root. Biol Pharm Bull. 1999;22(10):1144–1146.

37. Choi YJ, Lee J, Ha SH, Lee HK, Lim HM, Yu S-H, Lee CM, Nam MJ, Yang Y-H, Park K, et al. 6,8-Diprenylorobol induces apoptosis in human colon cancer cells via activation of intracellular reactive oxygen species and p53. Environ Toxicol. 2021;36(5):914–925.

38. Shao X, Chen X, Wang Z, Zhu C, Du Y, Tang D, Ji S. Diprenylated flavonoids from licorice induce death of SW480 colorectal cancer cells by promoting autophagy: activities of lupalbigenin and 6,8-diprenylgenistein. J Ethnopharmacol. 2022;296:115488.

39. Ballance S, Sahlstrøm S, Lea P, Nagy NE, Andersen PV, Dessev T, Hull S, Vardakou M, Faulks R. Evaluation of gastric processing and duodenal digestion of starch in six cereal meals on the associated glycaemic response using an adult fasted dynamic gastric model. Eur J Nutr. 2013;52(2):799–812.

40. Wallace BD, Wang H, Lane KT, Scott JE, Orans J, Koo JS, Venkatesh M, Jobin C, Yeh L-A, Mani S, et al. Alleviating cancer drug toxicity by inhibiting a bacterial enzyme. Science. 2010;330(6005):831–835.

41. Şöhretoğlu D, Sari S, Özel A, Barut B. α-Glucosidase inhibitory effect of *Potentilla astracanica* and some isoflavones: inhibition kinetics and mechanistic insights through in vitro and in silico studies. Int J Biol Macromol. 2017;105(Pt 1):1062–1070.